AIAA SciTech Forum
6-10 January 2020, Orlando, FL
AIAA Scitech 2020 Forum

10.2514/6.2020-1581

DNS investigation of laminar-to-turbulent transition with favorable pressure gradient: effects of surface imperfections

Daniel J. Wise*, Vinh-Tan Nguyen† and Kun Ting Eddie Chua‡
*Institute of High Performance Computing, A*STAR, 1 Fusionopolis Way, Connexis North #16-16, Singapore 138632*

Quoc Viet Nguyen§, Thirukumaran Nadesan¶ and Yongdong Cui‖
Temasek Laboratories, National University of Singapore, Engineering Drive 1, #09-02, Singapore 117411

Direct Numerical Simulations (DNS) have been performed of *a)* a flat-plate zero pressure gradient boundary layer and *b)* a flat-plate favorable pressure gradient boundary layer, using the numerical code NEK5000. The simulations are validated against analytical solutions and literature data in the laminar, transitional and turbulent regions. Surface imperfections in the form of a forward and backward facing step of varying heights have been implemented and simulated. Wind tunnel experiments have also been performed of a flat-plate zero pressure gradient boundary layer. Hot-wire measured velocity profiles indicate that the flow obeys the Blasius solution in the laminar region, and transition has been observed via interrogation of the hot-wire data. Both numerical and experimental results show that the introduction of step advances the location of transition onset. From the DNS, we find that for small step heights (less than 25% of the inlet boundary layer height), increasing pressure gradient by increasing the Falkner-Skan wedge angle delays the the onset of transition. However, the presence of significant step (50% of the inlet boundary layer height) negates the effect of pressure gradient, and the location of transition onset stagnates despite an increase in the Falkner-Skan parameter. Analysis of the longitudinal power spectrum shows that the growth of a sub-harmonic mode is enhanced with increasing step height.

I. Nomenclature

U_∞	=	Free-stream velocity
δ^*_{in}	=	displacement thickness of the inlet velocity profile
δ^*_{o}	=	displacement thickness of the outlet velocity profile
$Re_{\delta^*_0}$	=	Reference Reynolds number
$Re_{\delta^*_i}$	=	Inlet Reynolds number
Tu	=	Turbulence intensity
u, v, w	=	Fluid velocity in the streamwise, wall-normal and spanwise directions respectively
L_i	=	Length of computational domain in the i-th direction
N_i	=	Mesh grid-size in the i-th direction
$\bar{u}$	=	Time-averaged velocity
u'	=	Fluctuating component of u
Re_x	=	Reynolds x number
Re_θ	=	Momentum thickness Reynolds number
$A_1, A_{1/2}$	=	Disturbance amplitudes of the blowing/suction trip
ω_0	=	Fundamental mode frequency of of the blowing/suction trip
ϕ	=	Phase difference between the fundamental and sub-harmonic modes of blowing/suction trip
f, g	=	Modulation functions

*Scientist, Fluid Dynamics department
†Senior Scientist, Fluid Dynamics department
‡Corresponding author, Scientist, Fluid Dynamics department, e-mail: eddie_chua@ihpc.a-star.edu.sg
§Senior Research Scientist, Experimental AeroScience group
¶Senior Research Scientist, Experimental AeroScience group
‖Senior Research Scientist (Deputy Head), Experimental AeroScience group

h, w = Height and width of forward and backward facing step
T^* = Fluid temperature
ν_∞ = Fluid kinetic viscosity
C_f = Skin-friction coefficient
β_H, θ_H = Falkner-Skan parameter and wedge angle

II. Introduction

Skin-friction drag contributes to around 40% of the total drag experienced by a typical commercial jet, and any reduction to this drag would result in significant economic and ecological savings for an airline. Skin-friction drag can be reduced in either of two ways: by delaying transition to turbulence, or by altering the dynamics of an already turbulent flow. In general, the energy expenditure required to maintain a laminar flow is much less than that required to alter an already turbulent flow, and as such engineers have increasingly concentrated their efforts towards the development of techniques to delay transition to turbulence.

There exist several means through which transition can be delayed, all of which succeed by operating on one or more of the boundary layer stability modifiers (i.e. on the pressure gradient, surface mass flux, or surface heat flux) [1]. Acting on these modifiers dampens the linear growth of disturbances within the boundary layer, which is the most effective way to increase the transition Reynolds number under flight conditions [2]. Natural laminar flow (NLF) technology exploits one of the stability modifiers - employing a favorable pressure gradient to minimize disturbance growth and maintain a laminar boundary layer over a greater extent of an aerodynamic surface. NLF technology has been observed to delay transition to turbulence on surfaces with low sweep angles (<20°), and demonstrated to be effective on general aviation aircraft [3] and on business jets [4]. It is likely that its application to commercial passenger jets is not far behind.

Although NLF technology is one of the more mature techniques for reducing skin-friction drag on an aircraft, there are still significant unknowns when it comes to its performance in off-design or 'real' conditions, for instance in the presence of surface heating or surface imperfections. Progress has been made in this respect in recent years, particularly in the case of surface heating. Laboratory experiments on an NLF airfoil have shown that surface heating has a negative effect on the transition Reynolds number [5], while the combined effects of having both a pressure gradient and a non-adiabatic surface were documented by Costantini et al. [6]. Costantini et al. [6] performed a thorough parametric investigation on the pressure gradient (via β_H) and the wall temperature ratio, finding that larger β_H and smaller wall temperature ratio increased the transition Reynolds number. It was shown that along with the delay in transition, the amplification rates of the Tollmien-Schlichting (TS) waves were also reduced by the favorable pressure gradients and the lower temperature ratios.

Another of Morkovin's stability modifiers is the presence of surface roughness, and there has been extensive work on the effect of this on transition. Some sort of surface roughness is unavoidable on practical NLF surfaces, being present in the form of isolated roughness elements, slits, undulating surfaces and step junctions. These kinds of imperfection are, in general, known to promote the growth of TS waves, eventually leading to nonlinear breakdown and laminar-turbulent transition [7]. Exceptions exist, and recent studies show that spanwise-periodic roughness elements can suppress the growth of TS waves, delaying or completely suppressing transition [8–10]. The effects of isolated roughness and forward-facing steps on transition have been examined by Xu et al. [11] and Xu et al. [12], respectively. In both cases the investigation strategy was a combination of linear stability analysis and direct numerical simulation (DNS). For the case of isolated roughness, Xu et al. [11] found that TS waves are amplified in the presence of local roughness, leading to premature transition. Interestingly, Xu et al. [12] discovered that a smooth forward-facing step can either have a stabilizing or de-stabilizing effect on the boundary layer, depending on its height with respect to the local boundary layer height.

Research into the effects of surface imperfection on the stability of a boundary layer can be roughly separated into three categories: *a)* attempting to find threshold parameters for the imperfection geometry beyond which transition occurs; *b)* attempting to incorporate the effect of the imperfection into the e^N method; and *c)* performing a parametric investigation on the effects of the imperfection on transition location. The second of these techniques has probably received the most attention [i.e 13–15]. To our knowledge, the only systematic study on the combined effects of pressure gradient and surface imperfection (in the form of a forward facing step) can be found in Costantini et al. [16], who performed a parametric investigation on β_H and the step height. They performed temperature-sensitive paint measurements which indicated that the transition location moved upstream as the step height increased, and moved downstream with increasing β_H. Additionally the increase in β_H also was seen to result in a boundary layer that was more sensitive to changes in the step geometry. Further research is therefore needed in this area to not only

determine whether other imperfection geometries have a similar effect on transition, but additionally to determine whether transition mechanisms are altered under different conditions.

In the present work, we investigate the effects of surface imperfections, as characterized by an isolated step, on transitional boundary layers under zero and favorable pressure gradient conditions. Our results are based on an analysis of wind tunnel experiments and validated direct numerical simulations (DNS). We describe the numerical and experimental methodologies in §III.A and §III.C, respectively. The results and discussion are presented in §IV. Finally, we describe our conclusions in §V.

III. Methodology

A. Direct Numerical Simulation

We investigate laminar-turbulent transition using DNS of zero pressure gradient (ZPG) and favorable pressure gradient (FPG) flat-plate boundary layers. The simulations are conducted using Nek5000 [17], which solves the incompressible Navier-Stokes equations using a spectral-element method [18]. The spectral-spectral element method allows for the simulation of complex geometries that are usually only accessible through finite-volume or finite-element methods, while retaining the accuracy of spectral methods.

In Nek5000, the computation domain is discretized via a high-order weighted residual Galerkin approximation on a global domain decomposed into a finite number of non-overlapping elements. Within each spectral element, the solution is expanded at the Gauss-Lobatto-Legendre (GLL) quadrature points with Lagrange interpolants of order N. For the cases in the present study, solutions are obtained using a polynomial order of N=8. For time discretization, k^{th} order backward difference schemes ($k = 2, 3$) are implemented in Nek5000 for unsteady problems. In the case of incompressible Navier-Stokes flows, splitting techniques are used for advancing solutions in time by applying implicit and explicit discretization to separate terms in the governing equations, also referred to as implicit-explicit discretization. In Nek5000, there are two splitting approaches: analytical splitting using fractional steps and discrete splitting applying directly on discrete equations. Depending on the types of splitting techniques, the pressure is approximated in P_N or P_{N-2} resulting in different formulations referred to as $\mathrm{P}_N\mathrm{P}_N$ or $\mathrm{P}_N\mathrm{P}_{N-2}$ in Nek5000. In this work, we use a fractional time-step with the $\mathrm{P}_N\mathrm{P}_N$ formulation.We further utilize variable time-stepping, thus reducing the computational cost by maximizing the CFL number within the range CFL<2. For each simulation, we obtain time-averaged quantities by averaging over instantaneous flow fields taken after a steady state was reached.

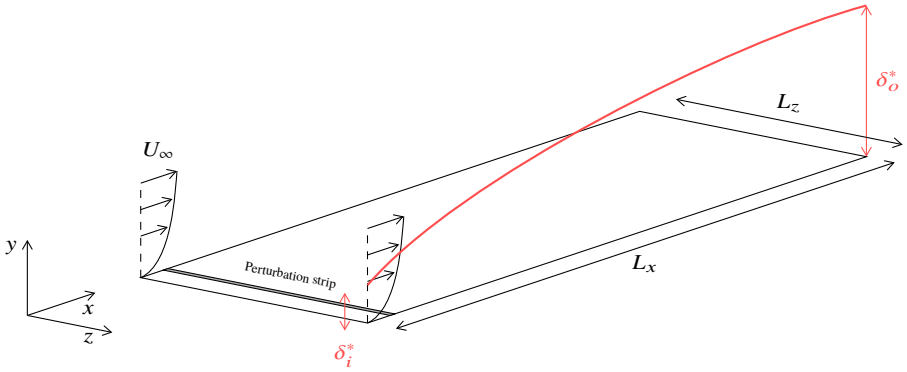

Fig. 1 A typical computational domain for DNS study of laminar-to-turbulent transition over a flat-plate, showing the simulation geometry and coordinate system implemented in the simulation code Nek5000. The perturbation strip near the inlet highlights the blowing and suction mechanism used to introduce disturbances into the simulation and induce transition. The red line illustrates the streamwise development of boundary layer thickness between the inlet and the outlet.

Fig. 1 shows a typical computational domain used for our simulations. All quantities are made dimensionless with the inlet boundary layer thickness δ^*_{in}, and the free-stream velocity U^*_∞. We apply a no-slip boundary condition (BC) to the flat plate, velocity inlet and outlet conditions at the streamwise boundaries, periodic BCs in the spanwise direction, and a free-shear BC at the top of the domain. Although it is assumed that the flow extends to an infinite distance in the wall-normal direction in the canonical zero pressure gradient boundary layer, this is not practical for simulation. As

such the flow domain is truncated in y, and an artificial boundary condition is applied at y=L_y, in the free-stream. This is given by the Dirichlet condition, $\mathbf{u}(y = L_y) = \mathcal{U}(y = L_y)$, where $\mathcal{U}(x, y)$ is the Blasius or Falkner-Skan base flow. In the case of the Falkner-Skan flow, the pressure gradient is imposed through the $\mathcal{U}(y = L_y)$ condition. The initial conditions are initialized with the Blasius solution in the ZPG case and the Falkner-Skan (FS) solution for the FPG case. At the inlet, the inflow condition is the Blasius (or FS) profile.

In all simulation cases, we introduce disturbances into the flow to induce transition. Following Huai et al. [19], we implement a wall-normal blowing and suction trip at x=50, as shown in Fig. 1. The perturbation strip adds bi-modal perturbations to the base flow, and extends throughout the spanwise direction. The wall-normal velocity of the blowing and suction strip is given by:

$$v(x, z, t) = A_1 f\,(x) \sin\left(\omega_0 t\right) + A_{1/2} f\,(x)\, g\,(z) \sin\left(\frac{\omega_0}{2} t + \phi\right), \tag{1}$$

In this formulation, the disturbances comprise two frequencies: a fundamental one (with frequency ω_0 and amplitude A_1), and a sub-harmonic disturbance (with frequency $\omega_0/2$ and amplitude $A_{1/2}$). The disturbances are modulated by the functions $f(x)$ and $g(z)$ as shown in Fig. 2. Disturbances of this nature are designed to match an earlier experiment of controlled sub-harmonic breakdown [20], and have been shown to successfully induce transition in the large-eddy simulations (LES) of [19].

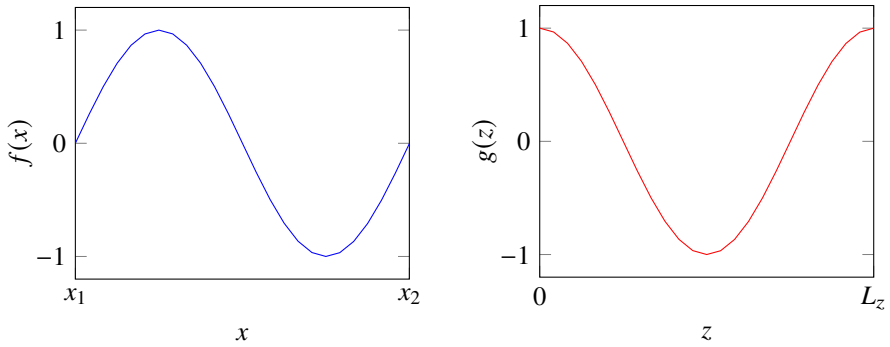

Fig. 2 Modulation functions used for the blowing/suction strip in the simulations.

We also examine the impact of small free-stream turbulence in the DNS. Following [21, 22], the free-stream turbulence consists of a combination of Fourier modes temporally and in the spanwise direction, and Orr-Sommerfeld and Squire modes in the vertical direction. This method has been applied to DNS of bypass transition, with turbulence intensities of 1% or more [e.g. 21–24]. In this work, we examine cases with Tu=0 and Tu=0.15%, the latter being similar to the free-stream turbulence measured in the wind tunnel (see §III.C).

We carry out various sets of flat-plate simulations in this work, summarized in Table 1. The first set (zpg_740) follows that of Huai et al. [19], which consists of a ZPG simulation with no surface imperfection. This simulation is performed with $Re_{\delta_0^*}$=740 and $Re_{\delta_{in}^*}$=605, which we use to validate the blowing and suction mechanism. Here the following trip parameters are used: ω_0=0.09136 rad s^{-1}, A_1=10^{-3} , $A_{1/2}$=10^{-5}, without free-stream turbulence (Tu=0). These results are validated against the experimental measurements of Kachanov and Levchenko [20] and discussed in Appendix §A.A.

The second set of simulations is performed on a smooth plate with no surface imperfections, while varying the Falkner-Skan angle θ_H in five steps between 0° (Blasius) and 5°. Here the parameters are chosen to match that of our wind tunnel experiments to be discussed in the next section. Due to increased Reynolds $Re_{\delta_0^*}$ compared to the zpg_740 case, the domain length is doubled to ensure that the boundary layer can completely transition to turbulent within the computational box. In this case, we utilized the following trip parameters: ω_0=0.01 rad s^{-1}, A_1=10^{-3} , $A_{1/2}$=0. An integral length scale for the free-stream turbulence of $5\delta_{\text{in}}^*$ is chosen to match the wind tunnel experiments.

To examine the impact of a isolated forward and backward-facing step, we conducted similar simulations while deforming the computational geometry to introduce isolated steps of width w=5. The simulations with a step height of h=0.25 can be identified with the suffix H025. Likewise, the simulations with a step height of h=0.5 can be identified with the suffix H05.

Finally, we have also considered cases with Tu=0.15%. These simulations can be identified with the additional suffix

Case	θ_H (°)	h	L_x	L_y	L_z	$N_x \times N_y \times N_z$	Tu (%)	$Re_{\delta_0^*}$
zpg_740	0	0	1000	50	50	$240 \times 24 \times 6$	0	740
zpg	0	0	2000	60	25	$420 \times 26 \times 6$	0	1126
fpg1.25	1.25	0	2000	60	25	$420 \times 26 \times 6$	0	1126
fpg2.5	2.5	0	2000	60	25	$420 \times 26 \times 6$	0	1126
fpg3.75	3.75	0	2000	60	25	$420 \times 26 \times 6$	0	1126
fpg5.0	5.0	0	2000	60	25	$420 \times 26 \times 6$	0	1126
zpg_H025	0	0.25	2000	60	25	$450 \times 25 \times 6$	0	1126
fpg1.25_H025	1.25	0.25	2000	60	25	$450 \times 25 \times 6$	0	1126
fpg2.5_H025	2.5	0.25	2000	60	25	$450 \times 25 \times 6$	0	1126
fpg3.75_H025	3.75	0.25	2000	60	25	$450 \times 25 \times 6$	0	1126
fpg5.0_H025	5.0	0.25	2000	60	25	$450 \times 25 \times 6$	0	1126
zpg_H05	0	0.5	2000	60	25	$450 \times 25 \times 6$	0	1126
fpg1.25_H05	1.25	0.5	2000	60	25	$450 \times 25 \times 6$	0	1126
fpg2.5_H05	2.5	0.5	2000	60	25	$450 \times 25 \times 6$	0	1126
fpg3.75_H05	3.75	0.5	2000	60	25	$450 \times 25 \times 6$	0	1126
fpg5.0_H05	5.0	0.5	2000	60	25	$450 \times 25 \times 6$	0	1126
zpg_Tu015	0	0	2000	60	25	$420 \times 26 \times 6$	0.15	1126
zpg_H025_Tu015	0	0.25	2000	60	25	$450 \times 25 \times 6$	0.15	1126
zpg_H05_Tu015	0	0.5	2000	60	25	$450 \times 25 \times 6$	0.15	1126
fpg2.5_Tu015	2.5	0	2000	60	25	$420 \times 26 \times 6$	0.15	1126
fpg2.5_H025_Tu015	2.5	0.25	2000	60	25	$450 \times 25 \times 6$	0.15	1126
fpg2.5_H05_Tu015	2.5	0.5	2000	60	25	$450 \times 25 \times 6$	0.15	1126

Table 1 Overview of simulation cases: respectively, Falkner-Skan angle, step height, domain length, domain height, domain width, grid size, free-stream turbulent intensity and reference Reynolds number.

Tu015, and are meant to match the turbulence intensity measured in the wind tunnel. In these cases, the free-steam turbulence intensity begins at 0.15% at the inlet and decays with streamwise distance, as shown in Fig. 3.

B. Laminar-turbulent discrimination

To distinguish between the laminar, transitional and turbulent regions of the flow, we rely on three measures. These are:

1) the turbulence intensity Tu,
2) the skin-friction $C_f \equiv \nu(d\bar{U}/dy)_{y=0}/(0.5U_\infty^2)$, and
3) the turbulence indicator function Γ.

Both Tu and C_f can determined straightforwardly from the flow field, while the calculation of Γ merits further discussion.

Our method for laminar-turbulence discrimination is based on that proposed by Nolan and Zaki [23], Marxen and Zaki [24], where we define a detector function $D \equiv v'_{rms} + w'_{rms}$ based on the rms of the fluctuating wall-normal and spanwise components and designed to pick out large velocity fluctuations. A low-pass filter in the form of Gaussian smoothing is then applied on the field D. Finally, we threshold the smoothed field using Otsu's method to obtain a binary indicator $\Gamma(x, y, z)$, which distinguishes between the laminar regions ($\Gamma = 0$) and the turbulent regions ($\Gamma = 1$). Otsu's method is a discrimination technique using in image processing which identifies the threshold by maximizing the inter-class variance between the two classes, i.e. between the non-turbulent and turbulent regions. We note that further applying this procedure to a database of instantaneous flow fields allows the probability that the flow at a point is turbulent, or *intermittency*, to be determined [23, 24]. We leave the study of the transitional region using the intermittency parameter to future work.

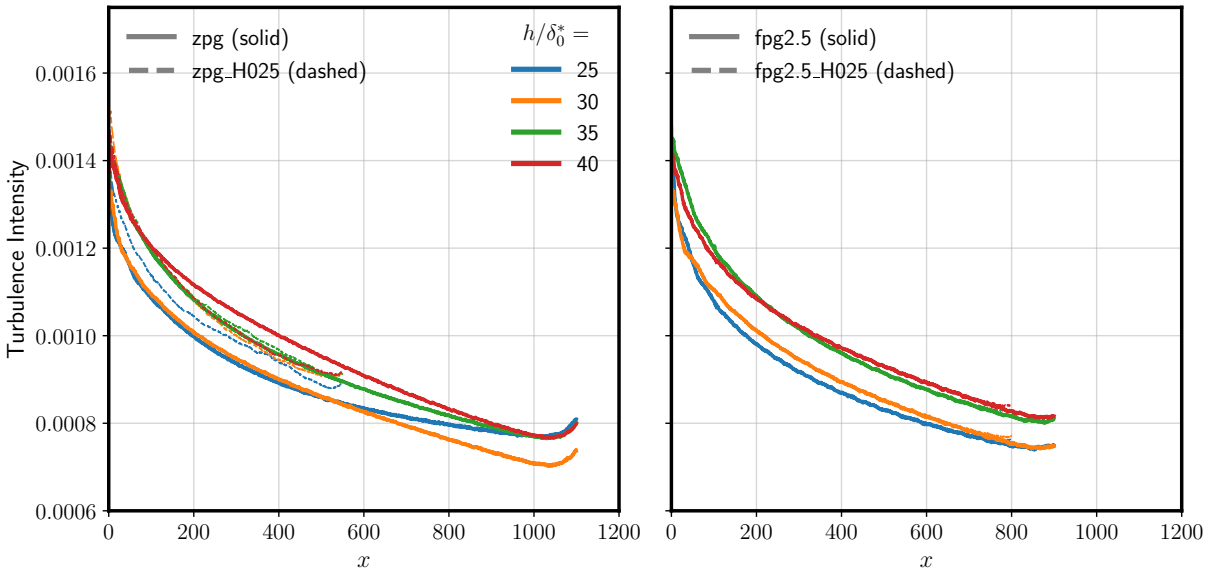

Fig. 3 Decay of free-stream turbulence intensity in the simulations with Tu=0.15% as a function of distance from the inlet for θ_H=0° (left) and θ_H=2.5° (right) in the laminar region. Solid and dashed lines show the results for h=0 and h=0.25, respectively. Due to the Orr-Sommerfeld and Squire modes, turbulence intensity is 0.15% at the inlet and decays with streamwise distance.

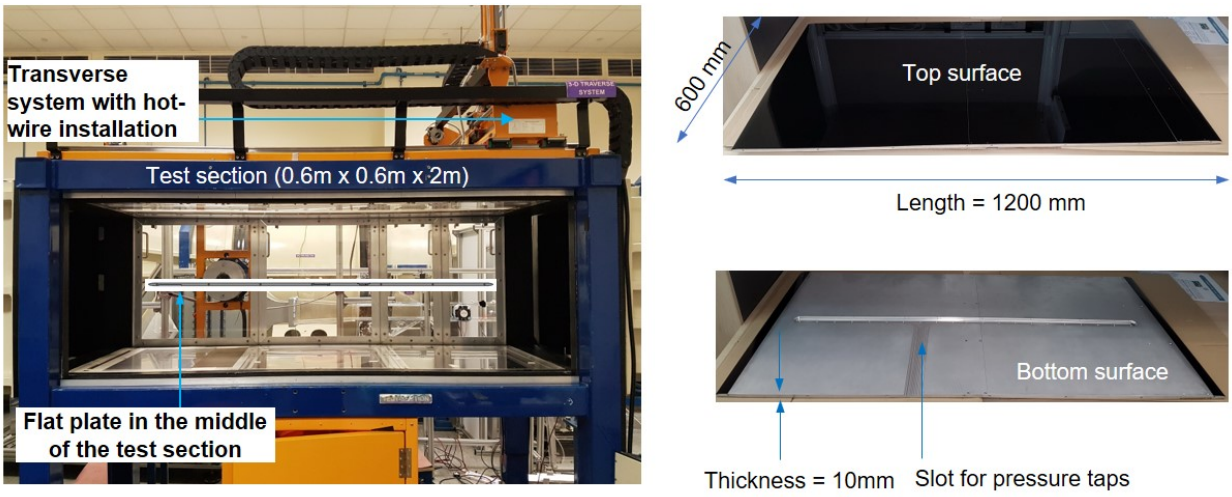

Fig. 4 Left: test-section of low-speed closed-loop wind tunnel used for experiments, with the flat plate installed. Right: Top and bottom surfaces of aluminum flat plate.

C. Wind tunnel Experiments

In order to validate the simulations, we also conduct experiments in the low-speed closed-loop wind tunnel at Temasek Laboratories, National University of Singapore where we investigate open boundary layer flow over an aluminum flat plate. The flat plate is constructed from two sections bolted together, with combined dimensions of 1200mm, 600mm, and 10mm in the streamwise, spanwise, and wall-normal directions respectively. The leading and trailing edges were designed as super-ellipses spanning 30 mm from both the ends of the plate. The top surface of the plate is painted to provide a smooth mirror-like surface and is mounted in the center of the test section, as shown in Fig .4.

Parameter	Units	Value
U^*_∞	m s^{-1}	35–41
ν^*_∞	kg $m^{-1}s^{-2}$	15.12 x 10^{-6}
T^*	°C	21

Table 2 Values for the nominal free-stream test conditions in the wind tunnel experiments.

Measurements relied on single-sensor hot-wire anemometry and were taken at the nominal conditions listed in Table 2. A miniature hot-wire probe with offset prongs and sensor perpendicular to the probe axis (DANTEC 55P15, for boundary-layer measurements) was operated in a constant-temperature anemometer mode using a DANTEC Streamline 90C10 module. Measurements of the time-averaged velocity, i.e. $\overline{u} = \int_0^T u dt$, and of the fluctuating component, i.e. $u' = u - \overline{u}$, were obtained along the spanwise and wall-normal directions and spanned respectively over distance of $\Delta z^* = \pm 100$ mm and $\Delta y^* = 1000$ mm. Traverse probe adjustments were exercised by automated stepper motors in $\Delta y^* = 0.1$ mm steps near the wall region and $\Delta y^* = 1$ mm (for laminar cases) and 5 mm (for turbulent cases) towards the outer edge boundary layer in the wall-normal direction. Steps were kept at $\Delta z^* = 5$ mm in the spanwise direction to eventually form a cross-sectional measurement plane with high near-wall resolution (where $\Delta y^* = 0.1$ mm). A DANTEC Streamline 90H02 flow unit connected to a high pressure line was used to conduct pre-run hot-wire calibrations. The temperature of the working fluid in the test-section was maintained close to the calibration temperature by use of a chiller unit. The chiller was operated when the test section temperature increased to over 0.5°C from the nominal calibration temperature of 21°C. Throughout the experiments, the test-section temperature was maintained within ±0.5°C from the nominal calibration temperature. The raw analog signals from the 90C10 Streamline module were passed through an individual low-pass anti-aliasing analog filter unit (eight-pole Butterworth at 3 KHz) before being digitized through an analog-to-digital data converter (NI PCI-6251). Data were sampled at 6 KHz (at 16 bits), yielding over $\approx 2^{16}$ samples per (x, y, z) location. The blockage effect due to the probe holder was on the order of 0.1% of the test section's area, and crossflow non-uniformities were within 0.1%. Further accounting for the uncertainties related to incoming flow conditions, the total error associated with the velocity measurements was estimated at less than 1.5%, and that with the turbulence intensity was estimated at less than 1.8%.

For the free-stream velocities investigated in the wind tunnel (U^*_∞ = 35–41 m s^{-1}, we measured Tu=u'_{rms}/U^*_∞=0.15%. The effect of a surface imperfection is introduced by installing an isolated step (i.e. forward and backward facing step) with a height of h=0.25 mm, width of 2.5 mm located at 110 mm from the leading edge. In terms of the displacement thickness, this corresponds to h=0.5δ^*_{in}. We conduct only experiments under zero-pressure conditions for comparisons with our simulations.

IV. Results

A. Experimental measurements

Experimentally, the impact of introducing a step on a flat plate can be seen in Fig. 5, which plots the turbulence intensity measured at $y \approx 1$ as a function of Re_x. In the smooth case (h=0, black circles), Tu begins to rise at $Re_x \approx 13 \times 10^5$, indicating in increase in flow fluctuations and the onset of transition. Introducing a step of height h=0.5 on the plate causes Tu to rise at $Re_x \approx 7 \times 10^5$, thus advancing upstream the onset of transition by $\Delta Re_x \approx 6 \times 10^5$.

Also shown in Fig 5 are the turbulence intensities from the corresponding Tu = 0.15% DNS runs (solid lines). Fig 5 shows reasonable agreement between experiments and DNS, which predict similar change in Re_x between the cases with and without a step. In both cases, we find that transition tends to occur further downstream in the DNS compared to the experiments. This is likely to due to other disturbances present in the boundary layer in the experiments not being accounted for in the DNS which leads to faster turbulent breakdown. These could include other sub-harmonics and harmonics in addition to the fundamental mode introduced by the blowing and suction trip.

Fig. 6 shows the wall-normal mean flow profiles in the presence of a step in the laminar region, at two streamwise locations. We compare the wind tunnel measurements (dots) with the corresponding DNS (zpg_H05_Tu015, dashed lines), where we have matched the streamwise locations using the closest Re_x values. Fig. 6 demonstrates that the mean laminar flow is not strongly perturbed by the step, and that there is excellent agreement between experiments and DNS.

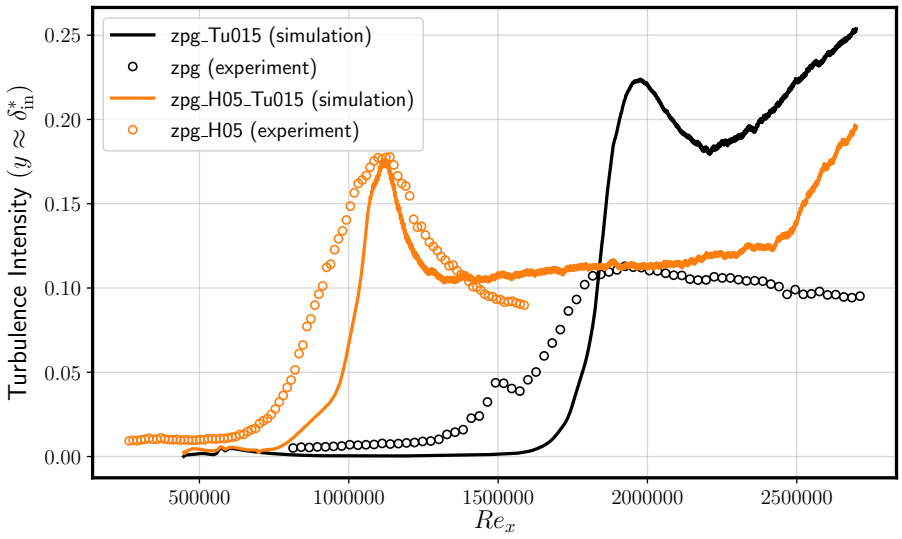

Fig. 5 Comparison of turbulence intensity as a function of Re_x between numerical simulations and experiments under zero pressure gradient conditions and turbulence intensity 0.15%. Results in black correspond to no surface imperfections while results in orange correspond to to a step with h = 0.5.

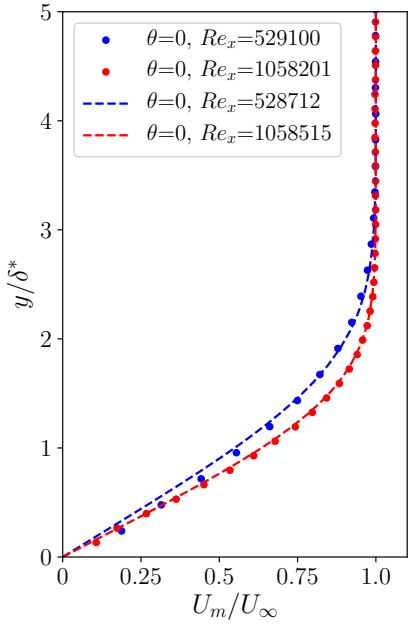

Fig. 6 Mean flow profiles in the laminar region with a step of height h=0.5 for the ZPG case. The DNS results and the corresponding experiments are shown as dashed lines and dotted symbols, respectively. Blue and red colors correspond to vertical profiles extracted at two streamwise locations. For DNS, the streamwise locations with the closest Re_x value to the experiments have been chosen.

B. Skin friction spatial distribution in DNS

Since the experimental measurements were only carried out for zero pressure gradient conditions, we turn to DNS to understand the effects of favorable pressure gradients in the presence of surface imperfections. Here we rely on the cases with Tu=0. For a qualitative overview of the simulation results, we visualize in Fig. 7 the spatial distribution of

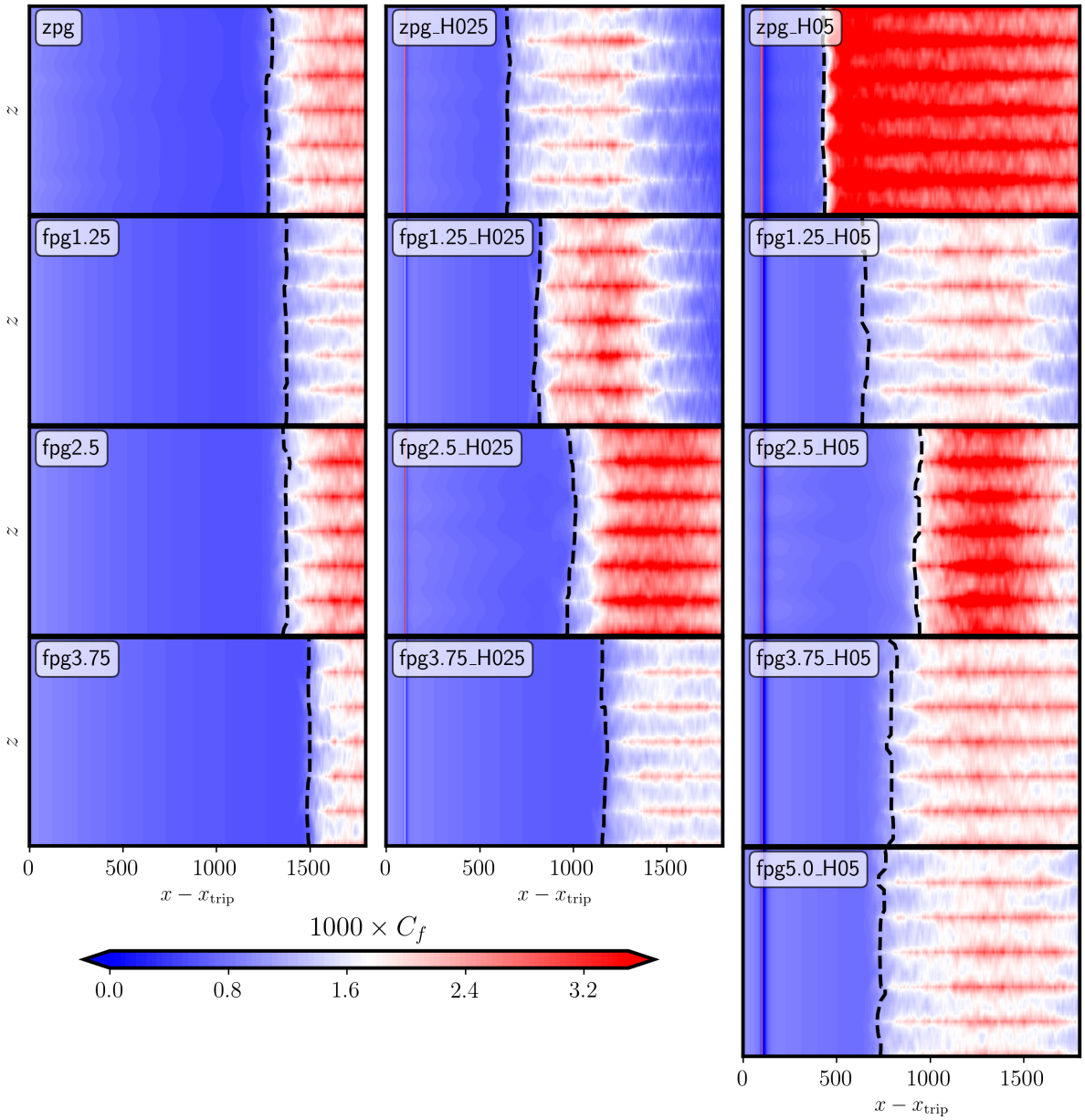

Fig. 7 Visualization of skin friction coefficients over the flat plate in the DNS simulations with Tu=0. The left column corresponds to flow over a smooth plate, i.e. without a step, while the right column corresponds to flow where an isolated step of height h=0.5 has been introduced. The fpg5.0 and fpg5.0_H025 cases are omitted since transition is not observed to occur within the simulation boxes.

the skin-friction coefficient on the flat-plate, for the cases where transition has been observed to occur. In the cases shown, the disturbances introduced by the perturbation strip and free-stream turbulence destabilize the flow, causing it to transition. Note that that the flow remains laminar in the fpg5.0 and fpg5.0_H025 cases, thus transition is not observed to occur within the simulation volume. Also denoted in Fig. 7 are boundaries of the indicator function Γ (dashed-lines) separating the regions where Γ=0 (upstream) and where Γ=1 (downstream). It can be seen that Γ=0 is associated with small C_f while Γ=1 is associated with large C_f and thus marks the boundary between laminar and turbulent flows.

In the H025 and H05 cases, the presence of the step induces local changes in C_f which can be observed at x=100. From Fig. 7, it is clear that both the pressure gradient and the presence of a step affects the breakdown to turbulence.

However, these two factors are not seen to influence the spanwise structure of the disturbances.

C. Spanwise-averaged statistics

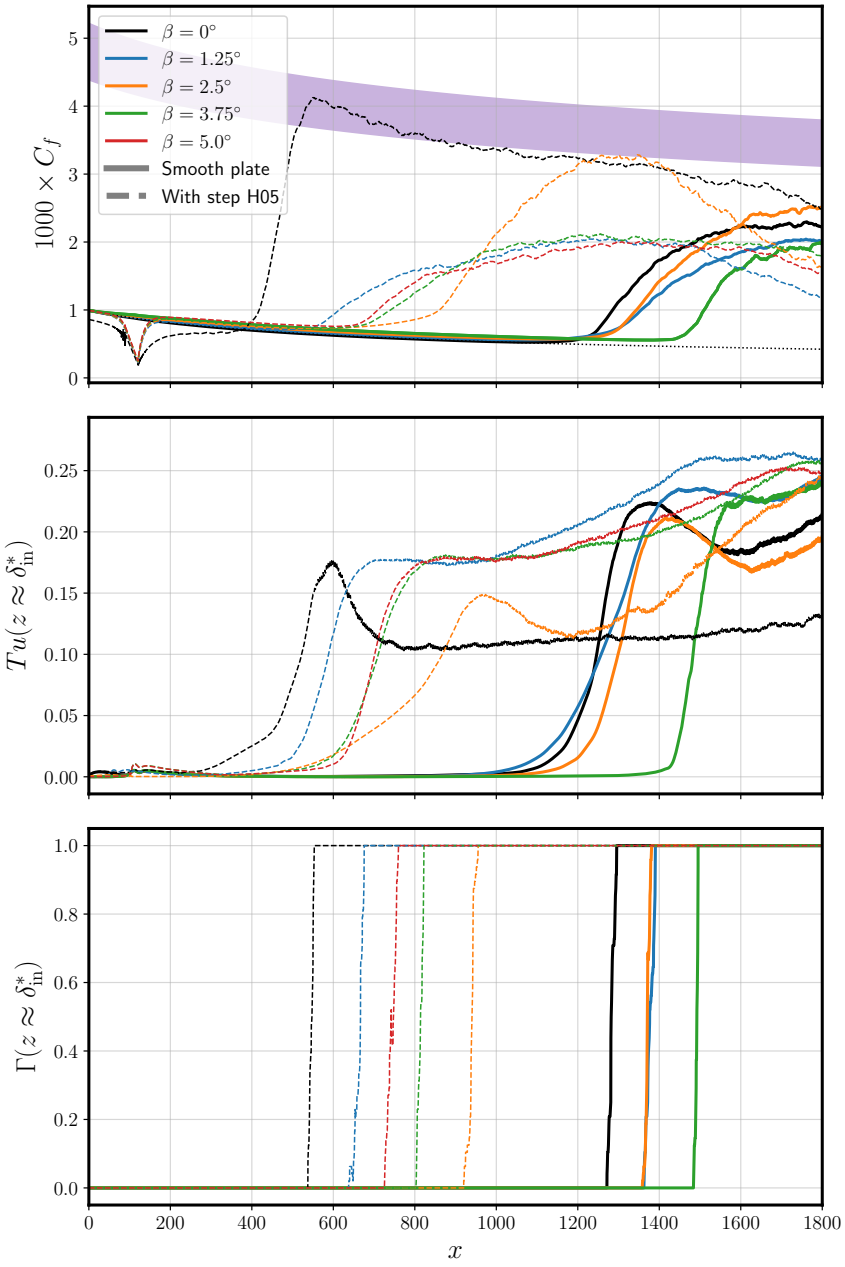

Fig. 8 Spanwise-averaged profiles from the simulations as a function of distance from the inlet in the simulations for a) the skin friction C_f (top), b) turbulence intensity Tu (middle), and c) turbulence indicator Γ (bottom).] Solid lines correspond to results over a smooth flat plate while dashed lines correspond to results with a step of height h=0.5. The dotted black line in the top panel denote the Blasius relation ($C_f = 0.664 Re_x^{-0.5}$) while the shaded region denote a range of turbulent solutions from literature.

We examine C_f in further detail by plotting its spanwise average as a function of x in the top panel of Fig. 8, concentrating on the smooth cases (solid lines) and the H05 cases (dashed lines). Colors correspond to the various

inclination angles. The Blasius relation for C_f ($C_f = 0.664 Re_x^{-0.5}$) is shown as the black dotted line, which agrees well with the θ_H=0° cases in the laminar regions. Near the inlet, the presence of the step at x=100 perturbs the flow in the step vicinity. However, C_f regains the Blasius (θ_H=0°) and Falkner-Skan values ($\theta_H > 0°$) shortly after the step.

Since the onset of transition is marked by an increase in C_f and thus a deviation from the Blasius and Falkner-Skan profiles, we define the streamwise location of transition onset by the minimum of the C_f vs x curve. Correspondingly, the transitional region is accompanied by a rise in the turbulence intensity, whose spanwise-average values at y=1 is shown in the middle panel of Fig. 8. Comparing C_f and Tu, we find that the departure of Tu from laminar precedes the start of transition (as defined using C_f). In this region, velocity fluctuations are starting to rise although the mean flow remains unaffected.

Finally, we show in the bottom panel of Fig. 8 the spanwise-averaged profiles of Γ profiles at a fixed height of y=1. Γ=1 marks where the flow is fully turbulent, thus Γ=0 includes both the laminar and transitional regions. The slope between Γ=0 and Γ=1 is steep since there is little spanwise variation in the location of the boundary (see Fig. 7).

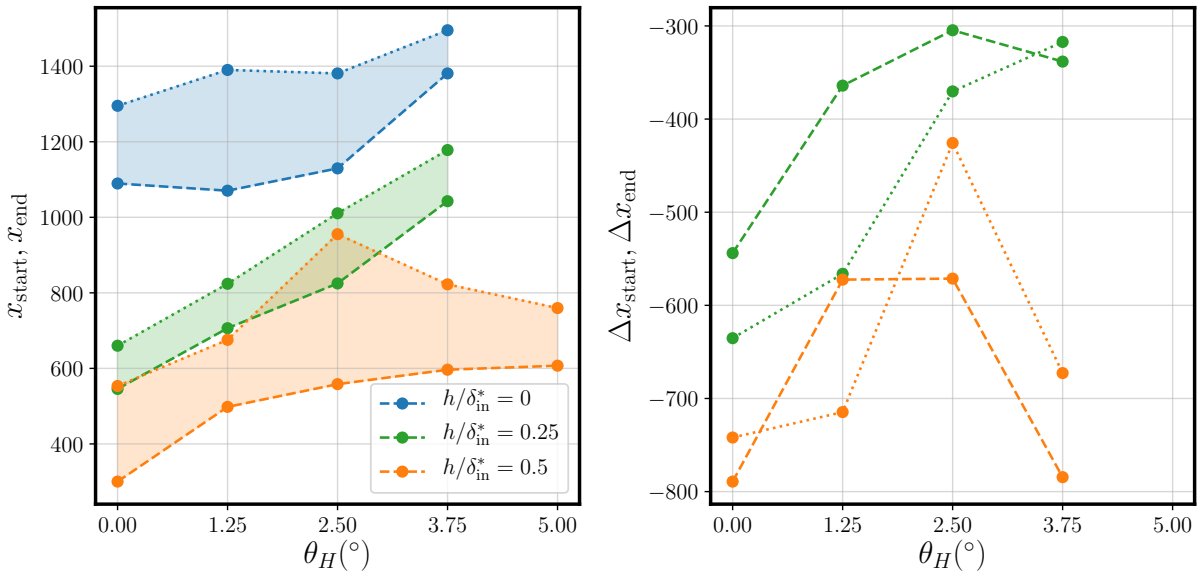

Fig. 9 Left: Location of transition onset (dashed) and the onset of fully turbulent flow (dotted) in the Tu=0 simulations as a function of θ_H. Blue, green and orange lines correspond no step, h=0.25, and h=0.25, respectively. Transition onset advances with increasing step height h. Increasing θ_H results in a more favorable pressure gradient and delays transition onset. For h=0.5, the step height is sufficient to induce transition within the simulation volume for θ_H=5°. For this step height, x_{start} saturates once the angle reaches θ_H=2.5°, after which increasing θ_H no longer delays transition onset. Right: Change in location of transition onset and full turbulence compared to the smooth h=0 case.

With the definitions of x_{start} and x_{end}, we summarize our results by plotting these quantities in Fig. 9 as a function of the angle θ_H for the cases with and without steps. For a given θ_H, increasing the step height advances the transition location upstream. In the case of θ_H=0°, the flow transitions significantly earlier, moving from $x \approx$1050 to 800 and 300 in the H025 and H05 cases respectively. For θ_H=5°, a step height of h=0.25 is insufficient to induce transition within the simulation volume whereas transition onset is observed at x=600 for h=0.5.

In general, increasing the Falkner-Skan angle i.e. having a more favorable pressure gradient, delays the onset of transition and the location of fully turbulent flow. For the h=0 and h=0.25 cases, the large favorable pressure gradient results in transition not being observed for θ_H=5°. When h=0.5, the location of transition onset stagnates at $x_{\text{start}} \approx$600 for $\theta_H \geq 2.5°$. With a step size of this height, it is no longer advantageous to increase the pressure gradient to bring about transition delay.

The effect of a step can be further observed in Fig. 10, which visualizes the spanwise averaged contours of the Reynolds stress $\overline{u'v'}$ for the three cases with θ_H=1.25°, in the vicinity of the step. In the fpg1.25 smooth plate case, the Reynolds stress caused by the free-stream turbulence is low. In the H025 and H05 cases, the step induces Reynolds

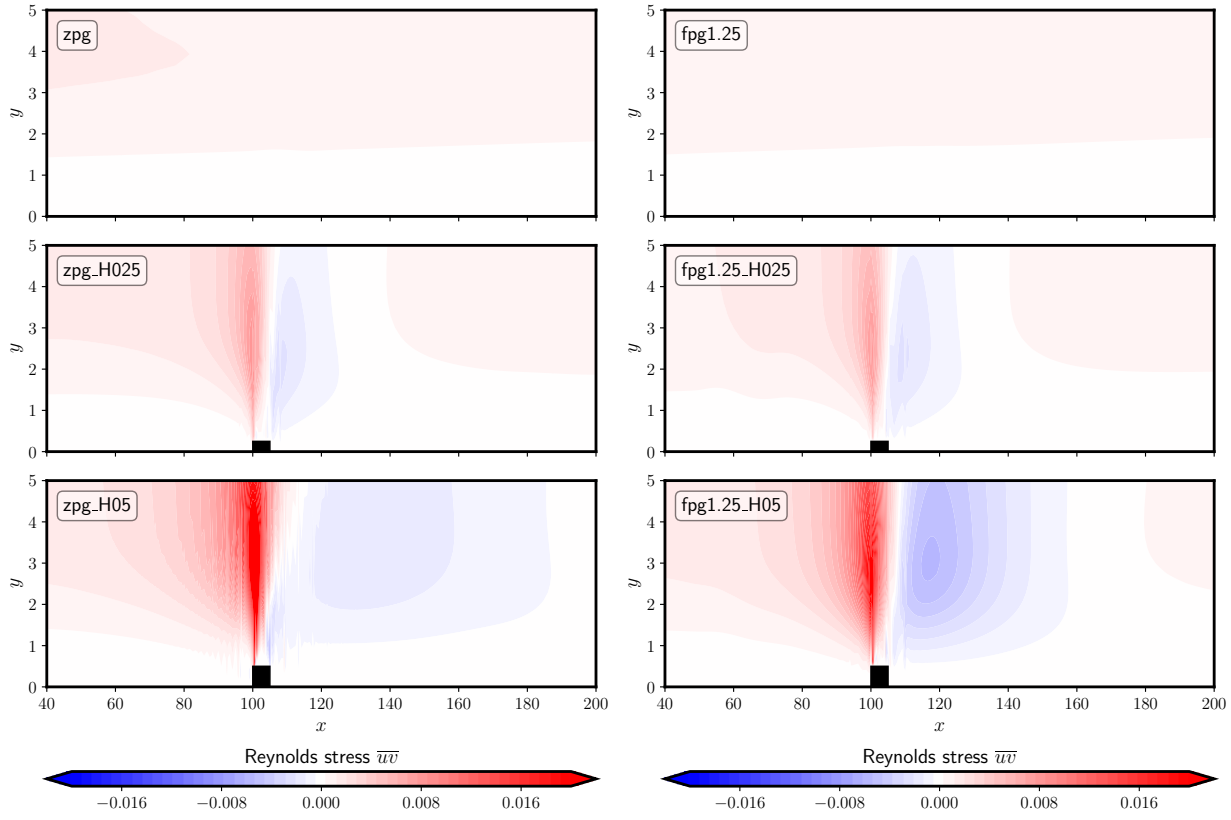

Fig. 10 Effect of steps on the spanwise averaged Reynolds stress $\overline{u'v'}$. Contours are visualized for the θ_H=0° (left column) and θ_H=1.25° (right column) cases. Top, middle and bottom rows correspond to h=0, 0.25 and 0.5 respectively. Steps induce Reynolds stresses in the flow that extend vertically beyond the step, and whose magnitudes are enhanced with increased step height.

stress that extend vertically beyond the step height. The magnitude of the Reynolds stresses is enhanced when the step height is increased from h=0.25 to h=0.5.

D. Power spectral density

In order to quantify the growth of disturbances and the effect of pressure gradient and steps, we compute the longitudinal power spectral density from the time-series of $u(t)$ obtained from the simulation snapshots. This is shown in Fig. 11 for four cases with Tu=0.15%. The spectra are extracted at y=1 and z=12.5 at various streamwise locations. Near the inlet at x=100, the power spectrum consists largely of a series of peaks, with a fundamental mode at k=0.02 Hz and other higher harmonics, a result of the free-steam modes introduced for non-zero turbulence intensity. Proceeding downstream, a growth of a sub-harmonic mode at $k \approx 0.01$ Hz is observed. Finally, where the flow is fully turbulent, the velocity power spectrum approaches Kolmogorov's law ($\propto k^{-5/3}$, red dashed line), characteristic of turbulent flow [25] in the inertial sub-range. With increasing step height, the downstream growth of the modes is more rapid, leading to an earlier onset of turbulence.

Interestingly, in the zpg_Tu015 case, an additional frequency mode at k=1.6×10^{-3} Hz is present at x=100, corresponding to ω_0=0.01 rad/s of the blowing and suction perturbation strip. This ω_0 peak is absent in the θ_H=2.5° cases. This is probably due to the combination of two factors: a) the interaction of the blowing and suction perturbations with the free-stream turbulence, and b) the favorable pressure gradient which suppresses the wall-normal propagation of the blowing and suction perturbations.

The power spectra for two of the Tu=0 cases are shown in Fig. 12, where we have chosen the two cases to facilitate comparison with the bottom row of Fig. 11. As expected, the peaks corresponding to the free-stream turbulence e.g. at k=0.02 Hz are absent in these cases. At x=100, the dominant frequency is that of the blowing and suction perturbation

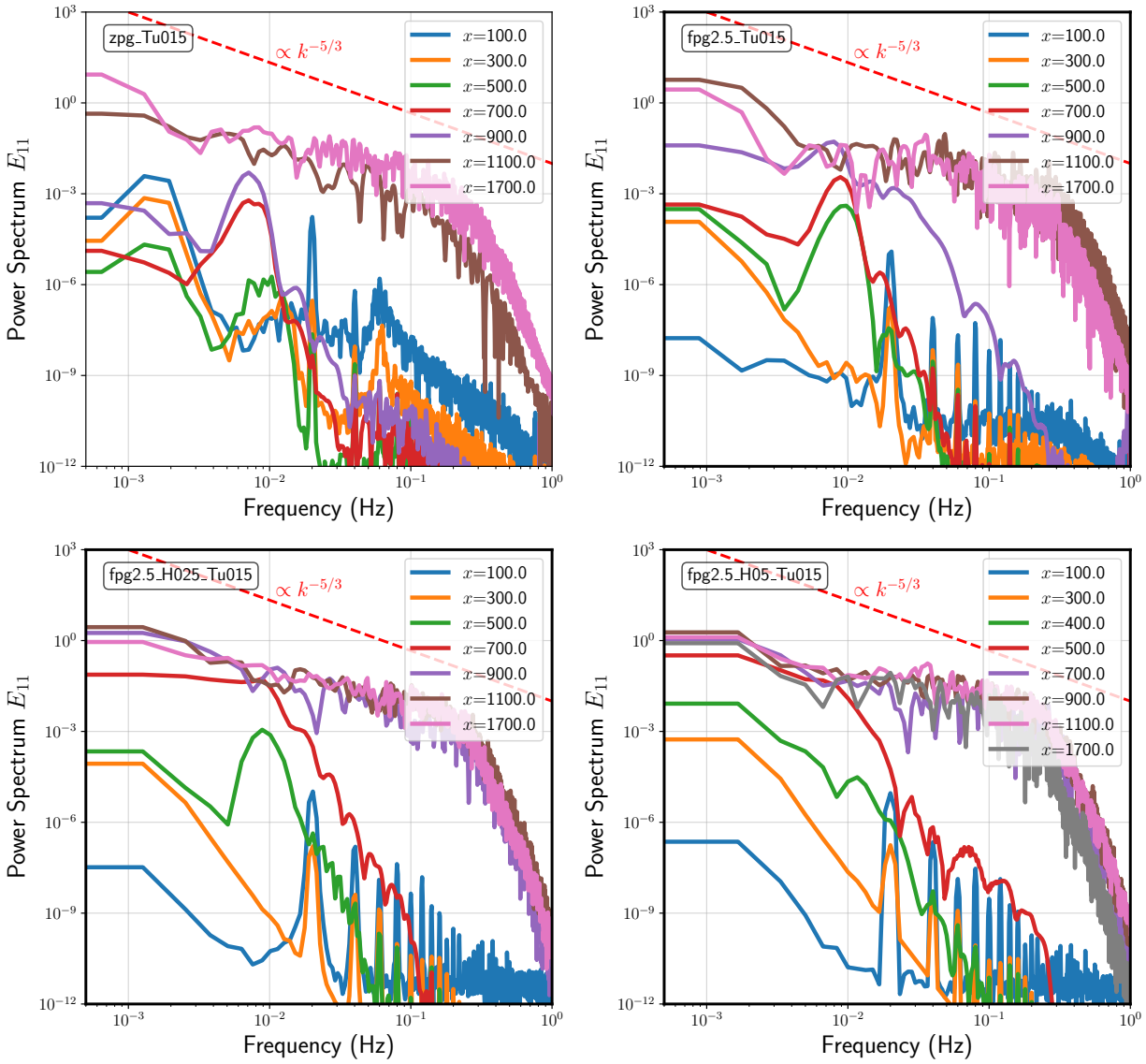

Fig. 11 Left: Longitudinal power spectrum for four Tu=0.15% simulation cases, obtained at y=1 and z=12.5 and at various streamwise positions. Also shown in red dashed lines is Kolmogorov's law ($\propto k^{-5/3}$). Most visible at x=100 for each case are frequency modes from free-stream turbulence, which has a dominant frequency here of k=0.02 Hz. The amplitude of a subdominant mode at $k \approx$0.01 Hz is observed to increase progressively downstream. Comparing the three θ_H=2.5° cases, we find that increasing the step height is accompanied by a more rapid growth of the sub-harmonic mode.

with ω_0=0.01 rad s^{-1}. Here, transition proceeds by the breakdown of this dominant mode promoting the growth of higher harmonics. We do not observe the growth of a sub-harmonic mode for this mechanism. Previous work on transition mechanisms have found sub-harmonic mode to be important e.g. in both N-type and K-type transitions [7]. For example in N-type transition, resonant interactions between the 3D sub-harmonic disturbances and the 2D fundamental mode drives the amplification of sub-harmonic frequency modes, as observed by the simulations of Huai et al. [19]. In these cases, sub-harmonic mode growth is absent due to the lack of a sub-harmonic mode in the blowing and suction trip ($A_{1/2} = 0$).

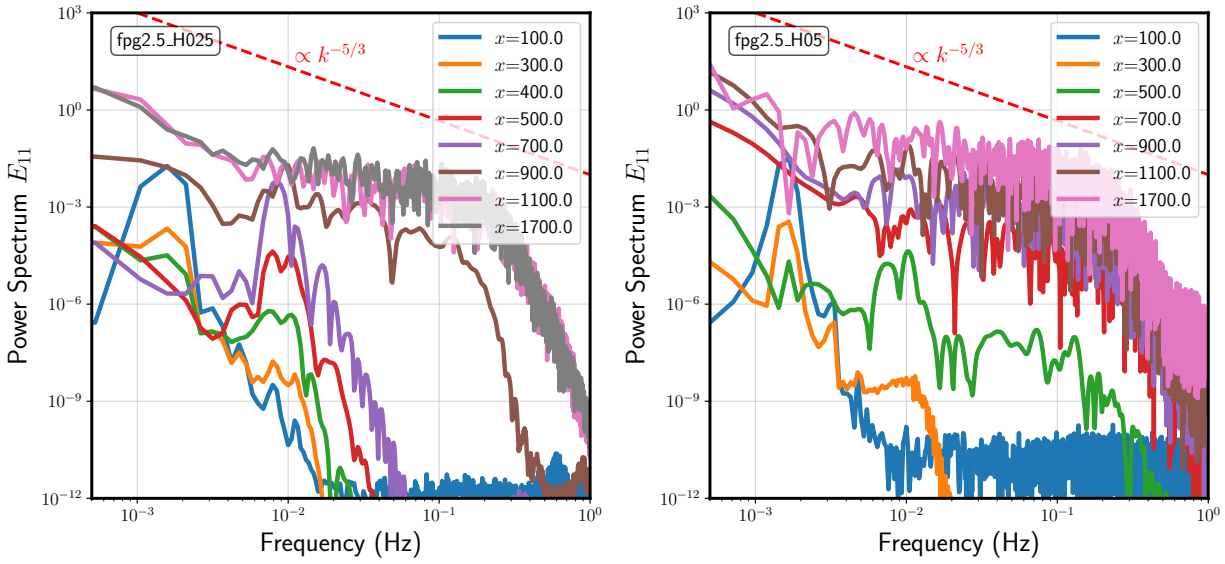

Fig. 12 Longitudinal power spectrum for two of the Tu=0 simulation cases, chosen here to facilitate comparison with Fig. 11. Due to the absence of free-stream turbulence, the dominant mode present at x=100 is that of the blowing and suction perturbation trip, with ω_0=0.01 rad/s = 1.6×10^{-3} Hz. Harmonics of this frequency is observed to grow downstream.

V. Conclusions

In this work, we have conducted direct numerical simulations to study the effect of surface imperfections and favorable pressure gradients on laminar-turbulent transition in an open boundary layer along a flat plate. The DNS are simulated with the Nek5000 code, where we have implemented free-stream turbulence and a blowing and suction trip to introduce perturbations in the flow and induce transition. Our main results are summarized as follows:

- Our DNS are validated against wind tunnel measurements for zero pressure gradient conditions, which demonstrate good agreement in the measured turbulent intensity profiles (Fig. 5). Both DNS and experiments highlight that introducing a forward and backward facing step of h=0.5 advances the location of transition onset.
- For sufficiently small step-heights, our DNS show that having a more favorable pressure gradient delays the onset of transition (Fig. 9). At θ_H=5°, the flow in both the h=0 and h=0.25 cases do not transition within the simulation box.
- However, having a more significant step-height negates the effect of increasing the pressure gradient. In our DNS with h=0.5, the streamwise location of transition onset stagnates at $x \approx 600$ despite increasing pressure gradient (Fig. 9).
- For a turbulence intensity of 0.15%, the downstream evolution of the power spectrum shows the growth of a sub-harmonic mode, which is amplified with increasing step height (Fig. 11)
- In the absence of free-stream turbulence, transition proceeds by the breaking down of the fundamental mode introduced by the blowing and suction trip (Fig. 12). In these cases, downstream evolution is not accompanied by sub-harmonic mode growth.
- We find that introduction of a step does not alter the spanwise structure of the flow (Fig. 7), but does induce Reynolds stress $\overline{u'v'}$ near the step.

Acknowledgments

The computational work for this article was performed on resources of the National Supercomputing Centre, Singapore (https://www.nscc.sg).

A. Appendix

A. Validation of blowing/suction trip

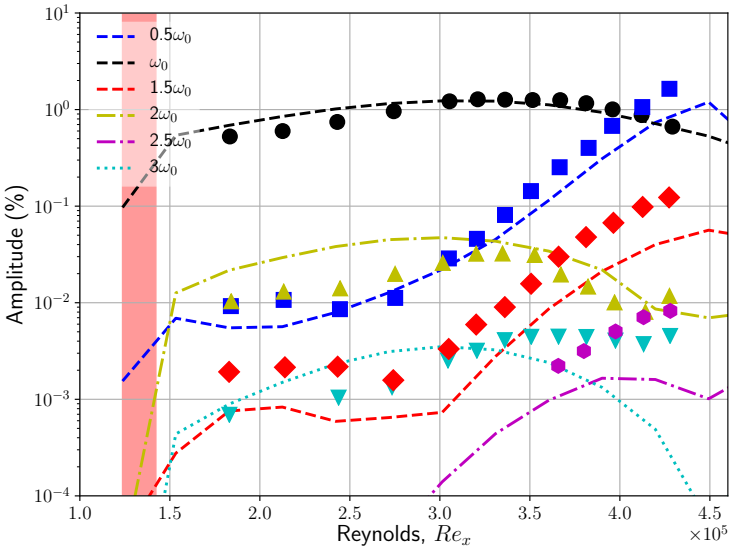

Fig. 13 Growth of DNS disturbance mode amplitudes and its harmonics as a function of Re_x (dashed lines) for the zpg_740 cases, compared with experimental data (symbols) from [20]. The red strip denotes the location of the blowing/suction trip.

We validate the blowing and suction trip (Eqn. 1) using the run zpg_740 with the experimental data from [20]. The parameters used (see §III.A) follow from the numerical work of [19]. Fig. 13 plots the amplitudes of various disturbance modes as a function of Reynolds Re_x. Following [19, 26], Our present DNS results (dashed lines) demonstrates excellent agreement with the experimental data (symbols) for the amplitudes of the fundamental and first sub-harmonic ($0.5\omega_0$) modes. The simulation under-predicts the amplitudes of the $1.5\omega_0$ and $2.5\omega_0$ modes and over-predicts that of the $2\omega 0$ mode, but captures the trend well. In this case, transition occurs at $Re_x \approx 420000$, where the sub-harmonic amplitude (blue) exceeds that of the fundamental mode (black).

References

[1] Morkovin, M., "Critical evaluation of transition from laminar to turbulent shear layers with emphasis on hypersonically traveling bodies," Tech. rep., Martin Marietta Corp Baltimore MD Research Inst. For Advanced Studies, 1969.

[2] Reshotko, E., "Boundary layer instability, transition and control," *32nd Aerospace Sciences Meeting and Exhibit*, 1994, p. 1.

[3] Holmes, B., Obara, C., and Yip, L., "Natural Laminar Flow Experiments on Modern Airplane Surfaces," *NASA Technical Paper*, Vol. 2256, 1984.

[4] George, F., "Piaggio Aero P180 Avanti II," *Business and Commerical Aviation*, Vol. 101, No. 3, 2007.

[5] Stock, H. W., "Wind tunnel–flight correlation for laminar wings in adiabatic and heating flow conditions," *Aerospace science and technology*, Vol. 6, No. 4, 2002, pp. 245–257.

[6] Costantini, M., Hein, S., Henne, U., Klein, C., Koch, S., Schojda, L., Ondrus, V., and Schröder, W., "Pressure gradient and nonadiabatic surface effects on boundary layer transition," *AIAA Journal*, 2016, pp. 3465–3480.

[7] Kachanov, Y. S., "Physical mechanisms of laminar-boundary-layer transition," *Annual review of fluid mechanics*, Vol. 26, No. 1, 1994, pp. 411–482.

[8] Saric, W. S., Carrillo, R. B., and Reibert, M., "Nonlinear stability and transition in 3-D boundary layers," *Meccanica*, Vol. 33, No. 5, 1998, pp. 469–487.

[9] Shahinfar, S., Sattarzadeh, S., Fransson, J., and Talamelli, A., "Revival of classical vortex generators now for transition delay," *Physical review letters*, Vol. 109, No. 7, 2012, p. 074501.

[10] Downs, R., and Fransson, J., "Tollmien–Schlichting wave growth over spanwise-periodic surface patterns," *Journal of Fluid Mechanics*, Vol. 754, 2014, pp. 39–74.

[11] Xu, H., Sherwin, S., Hall, P., and Wu, X., "The behaviour of Tollmien–Schlichting waves undergoing small-scale localised distortions," *Journal of Fluid Mechanics*, Vol. 792, 2016, pp. 499–525.

[12] Xu, H., Lombard, J., and Sherwin, S., "Influence of localised smooth steps on the instability of a boundary layer," *Journal of Fluid Mechanics*, Vol. 817, 2017, pp. 138–170.

[13] Perraud, J., Arnal, D., Seraudie, A., and Tran, D., "Laminar-turbulent transition on aerodynamic surfaces with imperfections," *ONERA: Tire a Part*, Vol. 13, 2004, p. 2004.

[14] Perraud, J., Arnal, D., and Kuehn, W., "Laminar-turbulent transition prediction in the presence of surface imperfections," *International Journal of Engineering Systems Modelling and Simulation 48*, Vol. 6, No. 3-4, 2014, pp. 162–170.

[15] Wang, Y., and Gaster, M., "Effect of surface steps on boundary layer transition," *Experiments in Fluids*, Vol. 39, No. 4, 2005, pp. 679–686.

[16] Costantini, M., Risius, S., Klein, C., and Kühn, W., "Effect of forward-facing steps on boundary layer transition at a subsonic Mach number," *New Results in Numerical and Experimental Fluid Mechanics X*, Springer, 2016, pp. 203–213.

[17] Fischer, P., Lottes, J., and Kerkemeier, S., "nek5000 Web page," , 2008. Http://nek5000.mcs.anl.gov.

[18] Patera, A., "A spectral element method for fluid dynamics: laminar flow in a channel expansion," *Journal of computational Physics*, Vol. 54, No. 3, 1984, pp. 468–488.

[19] Huai, X., Joslin, R., and Piomelli, U., "Large-eddy simulation of transition to turbulence in boundary layers," *Theoretical and computational fluid dynamics*, Vol. 9, No. 2, 1997, pp. 149–163.

[20] Kachanov, Y., and Levchenko, V., "The resonant interaction of disturbances at laminar-turbulent transition in a boundary layer," *Journal of Fluid Mechanics*, Vol. 138, 1984, pp. 209–247.

[21] Jacobs, R., and Durbin, P., "Simulations of bypass transition," *Journal of Fluid Mechanics*, Vol. 428, 2001, pp. 185–212.

[22] Brandt, L., Schlatter, P., and Henningson, D., "Transition in boundary layers subject to free-stream turbulence," *Journal of Fluid Mechanics*, Vol. 517, 2004, pp. 167–198.

[23] Nolan, K. P., and Zaki, T. A., "Conditional sampling of transitional boundary layers in pressure gradients," *Journal of Fluid Mechanics*, Vol. 728, 2013, p. 306–339. doi:10.1017/jfm.2013.287.

[24] Marxen, O., and Zaki, T. A., "Turbulence in intermittent transitional boundary layers and in turbulence spots," *Journal of Fluid Mechanics*, Vol. 860, 2019, p. 350–383. doi:10.1017/jfm.2018.822.

[25] Pope, S., *Turbulent Flows*, Cambridge University Press, 2000.

[26] Kachanov, Y. S., "Physical mechanisms of laminar-boundary-layer transition," *Annual review of fluid mechanics*, Vol. 26, No. 1, 1994, pp. 411–482.